Langmuir

Article

pubs.acs.org/Langmuir

Improved Electrocatalytic Ethanol Oxidation Activity in Acidic and Alkaline Electrolytes Using Size-Controlled Pt−Sn Nanoparticles

Samuel St. John,[†] Punit Boolchand,[‡] and Anastasios P. Angelopoulos*,[†]

[†]Chemical Engineering Program School of Energy, Environmental, and Biological & Medical Engineering and [‡]Computer and Electrical Engineering Program School of Electronic and Computing Systems, University of Cincinnati, Cincinnati, Ohio 45221, United States

ABSTRACT: The promotion of the electrocatalytic ethanol oxidation reaction (EOR) on extended single-crystal Pt surfaces and dispersed Pt nanoparticles by Sn under acidic conditions is well known. However, the correlation of Sn coverage on Pt nanoparticle electrocatalysts to their size has proven difficult. The reason is that previous investigations have typically relied on commercially difficult to reproduce electrochemical treatments of prepared macroscopic electrodes to adsorb Sn onto exposed Pt surfaces. We demonstrate here how independent control over both Sn coverage and particle size can yield a significant enhancement in EOR activity in an acidic electrolyte relative to previously reported electrocatalysts. Our novel approach uses electroless nanoparticle synthesis where surface-adsorbed Sn is intrinsic to Pt particle formation. Sn serves as both a reducing agent and stabilizing ligand, producing particles with a narrow particle size distribution in a size range where the mass-specific electrocatalytic activity can be maximized (ca. 1−4 nm) as a result of the formation of a fully developed Sn shell. The extent of fractional Sn surface coverage on carbon-supported Pt nanoparticles can be systematically varied through wet-chemical treatment subsequent to nanoparticle formation but prior to incorporation into macroscopic electrodes. EOR activity for Pt nanoparticles is found to be optimum at a fractional Sn surface coverage of ca. 0.6. Furthermore, the EOR activity is shown to increase with Pt particle size and correlate with the active area of available Pt (110) surface sites for the corresponding Sn-free nanoparticles. The maximum area- and mass-specific EOR activities for the most active catalyst investigated were 17.9 $\mu A/cm^2_{Pt}$ and 12.5 A/g_{Pt}, respectively, after 1 h of use at 0.42 V versus RHE in an acidic electrolyte. Such activity is a substantial improvement over that of commercially available Pt, Pt−Sn, and Pt−Ru alloy catalysts under either acidic or alkaline conditions.

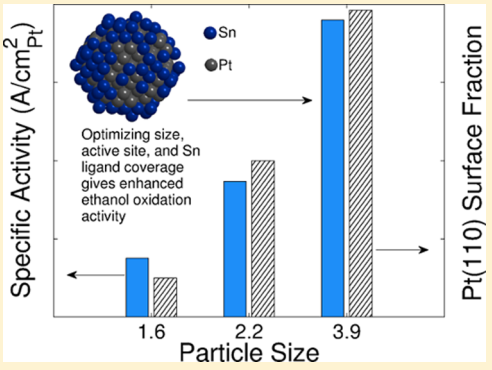

INTRODUCTION

Direct ethanol fuel cells (DEFCs) offer the potential of the high-energy-density production of electricity. Compared to hydrogen, ethanol is attractive as a portable fuel source for many reasons: (1) an energy density of 8.1 compared to 0.42 kW h/kg for hydrogen and 6.1 for methanol;[1] (2) liquid transportation and storage at ambient pressure as opposed to the pressurized gas requirements of hydrogen; and (3) the potential to use bioderived sources such as sugar cane. A continuing challenge to the commercialization of DEFCs is the sluggish ethanol oxidation reaction (EOR) due to the difficulty of cleaving the C−C bond on precious metal Pt catalysts.[2] The Pt surface can also become rapidly contaminated with adsorbed CO (CO_{ads}) and other intermediates during oxidation. Acetaldehyde is the chief partial oxidation product on Pt-only catalysts, which can irreversibly bind to the catalyst surface and poison further reaction.[1,3] Furthermore, the sulfuric acid electrolyte has previously been shown to impede electrocatalytic oxygen reduction reaction (ORR) activity on the extended Pt(111) surface,[4,5] and this site is hypothesized to dominate both ORR and EOR activity for dispersed Pt nanoparticles.[4,6] However, a systematic investigation has yet to be performed on how the Pt nanoparticle surface structure (e.g., the relative distribution of (111), (110), and (100) sites on nanocrystalline surfaces) is correlated to EOR activity.

Alkaline conditions and the use of hydroxide anion transport membranes have attracted increasing interest as a means of mitigating interference by irreversibly bound surface species in the case of EOR.[7] However, more recent work has shown that electrolyte effects on the ORR activity of dispersed Pt nanoparticles are not as significant as on extended surfaces.[8] Detailed adatom investigations[9] have demonstrated that this behavior is due to the fact that highly dispersed Pt nanoparticles contain disordered surfaces that are incapable of supporting Pt(111) terraces and that activity is instead dominated by the presence of Pt(110)-like surface sites. The degree to which the electrocatalytic activity is inhibited in sulfuric acid direct ethanol fuel cells due electrolyte adsorption is therefore uncertain. In addition, the impact of particle size on EOR under either alkaline or acidic conditions in the presence of a CO_{ads} oxidation promoter (e.g., Sn or Ru) is not presently known. We wish here to determine how the recently observed increase in the fraction of Pt(110) sites relative to inactive

Received: September 25, 2013
Revised: December 2, 2013
Published: December 6, 2013

   dx.doi.org/10.1021/la403704w | Langmuir 2013, 29, 16150−16159

lower-coordination sites with increasing Pt particle size[9] is correlated to EOR activity under both alkaline and acidic conditions.

Sn has been shown to promote the oxidation of EOR intermediates at low potentials under acidic conditions by activating water and thereby keeping the surface free of CO_{ads} (e.g., acetaldehyde) on extended Pt surfaces.[3,10] A great deal of experimental work concerning the promotional effect of Sn-containing catalysts for alcohol oxidation has been done on polycrystalline and basal plane surfaces (both the Pt−Sn bulk alloy and bulk Pt onto which metallic Sn has been initially deposited)[11−21] and on Pt−Sn nanoparticle alloys.[10,15,17,22−31] The theoretical mechanism of water activation by Sn for CO_{ads} oxidation is well established.[20,21,32−40] Much of the research investigating the promoting affect of Sn has tended toward the effect with Sn alloys. However, several authors have investigated the promoting ability of irreversibly adsorbed Sn on Pt surfaces.[14,17,20,21] Previous investigations of the promotional effect of irreversibly bound Sn on Pt surfaces for EOR have all relied on electrochemical Sn adsorption. This contrasts with our present work wherein surface-adsorbed Sn is intrinsic to Pt nanoparticle synthesis. By not relying on the postsynthesis processing of prepared electrodes, our method provides a more straightforward transition to commercially viable supported electrocatalysts.

Several reports have appeared that investigate the effect of SnO_2 nanoparticles in close proximity to Pt and Pt-M alloy active sites.[3,12,41] Some authors have also shown that the use of ternary electrocatalysts where Pt−Rh alloy nanoparticles are deposited onto carbon-supported SnO_2 nanoparticles has led to the direct oxidation of ethanol toward CO_2 through C−C bond cleavage at new active sites in the junction between Pt−Rh and SnO_2 nanoparticles.[2,41−44] The role of SnO_2 in these studies is shown to be primarily to keep the surface sites capable of cleaving the C−C bond free from adsorbed intermediates.[44] Optimum EOR activity has been observed as the bulk SnO_2 concentration in the nanoparticles is varied in this ternary catalyst system.[42] However, the optimal Sn surface coverage on dispersed Pt nanoparticle surfaces for EOR activity is not known. Our work here represents the first step toward controlling Sn surface coverage on noble metal nanoparticles to optimize the active site distribution for the removal of adsorbed intermediates under acidic conditions.

We have recently developed a nanoparticle synthesis method not previously investigated for EOR that is uniquely suited to the study of the promotional effect of Sn on the EOR in highly dispersed Pt systems.[45] Our work builds on that by Mukerjee et al.[14,17] and Du et al.[3] to investigate the promotion of CO_{ads} removal from the surface of Pt nanoparticles by adsorbed Sn. Our synthesis involves the stabilization and growth termination of Pt nanoparticle cores by Coulombic repulsion of the $SnCl_3^-$ ligands that remain on the nanoparticle surface following Pt reduction. The ligands are converted to SnO_2 in subsequent chemical washes during electrostatic assembly onto carbon supports.[45−47] We will use this novel electrocatalyst preparation method to show how systematic control over the underlying geometric structure of the Pt nanoparticle active site distribution as well as Sn surface coverage can be used to optimize the EOR activity.

In our previous work, we have shown how stannous chloride may be used as both a reducing and stabilizing ligand to form monodisperse Pt nanoparticles in a stable suspension over a precisely controlled size range that is critical to optimizing nanoparticle mass-normalized electrocatalytic activity for the oxygen reduction reaction (ORR).[45,47] The synthesis scheme produces stable particles that span the atomic cluster-to-nanocrystal transition (ca. 0.5 − 3 nm) with less than a 10% standard deviation at each particle size. Control is achieved by simply varying the Sn/Pt ratio during synthesis.[45,47] The resulting nanoparticles possess high electrocatalytic oxygen reduction reaction (ORR) activity relative to nanocrystals and commercial Pt systems[45−47] by maximizing the available Pt(110) and Pt(311) five-coordinate surface sites.[9] The stabilizing ligand can be converted from its chloride form to its oxide. The oxide has been shown to form labile oxygen species that have been shown to be responsible for the electrocatalytic activity of Sn for the methanol oxidation reaction (MOR) and CO_{ads} removal.[17]

We will demonstrate here why highly dispersed nanoparticles exhibit significant variations in EOR mass activity with particle size and Sn content. Optimum Sn coverage will be shown to be approximately 60% and similar to that in extended single-crystal surface studies conducted by El-Shafei et al.[18] and Sobkowski et al.[19] where the Pt(110) surface is hypothesized to be the most active.[48,49] However, for the first time in the field, the EOR activity is correlated with the changing surface distribution of Pt active sites with increasing particle size under both acidic and alkaline conditions. The activity will be shown to increase with the availability of (110) and (311) five-coordinate active sites relative to that for sites of lower coordination. The synthesis technique demonstrated here may be extended to a great variety of noble metal alloys and represents a potential avenue for developing highly active catalysts for alcohol oxidation in various electrolytes.

EXPERIMENTAL METHODS

Pt Nanoparticle Synthesis. The nanoparticle synthesis method[45−47] is analogous to one described originally by Cohen and West for the synthesis of Pd nanoparticles;[50] we briefly describe that method here. Equal-volume (100 mL) solutions of $SnCl_2$ in 7.5 M HCl are mixed rapidly while boiling with solutions of 0.03 M $PtCl_4$ in 7.5 M HCl. The particles investigated here were synthesized using atomic Sn/Pt ratios in the synthesis solution of 2.5, 3, and 9. The combined solutions are boiled under reflux for 1 h, after which time heat is removed and the nanoparticles are allowed to cool overnight. Both solutions are deoxygenated with nitrogen (purity plus ultra-high-purity 99.999%) prior to mixing and during reaction. The particle size, distribution, and colloidal stability are controlled by $SnCl_3^-$ ligands that bond nonspecifically to the surface via the capping effect of the colloid-stabilizing $SnCl_3^-$ ligand. The particle size distribution is limited to about 10% for all nanoparticles synthesized here as determined using high-angle annual dark-field scanning transmission electron microscopy (HAADF-STEM).

LbL Assembly and Pt−C Ink Fabrication. The size-controlled Pt nanoparticles synthesized here are assembled on a carbon support using electrostatic assembly[45,47] to make Pt−C inks. These inks are then cast onto rotating disk electrodes for activity assessment. As a summary, a cationic polyacrylamide (acrylamide/β-methacryloxyethyltrimethylammonium-methyl sulfate copolymer, obtained commercially as Superfloc C-442 from Cytec Industries Inc.) was mixed with a high-surface-area Vulcan Carbon XC-72 support (Cabot) from a 0.6 g/L suspension in 0.1 M H_2SO_4. The materials were mixed and sonicated for 30 min and then centrifuged and washed three times with DI water to remove any residual polymer. The polymer-coated carbon was resuspended in a 50% mixture of IPA and water via sonication. Pt nanoparticles were added in excess to the resuspended cationic-polymer-coated carbon and sonicated for 30 min. The sample mixture was sonicated for 30 min, centrifuged, and rinsed with 0.1 M NaOH for 10 min. The samples were centrifuged, triply washed with DI

dx.doi.org/10.1021/la403704w | Langmuir 2013, 29, 16150−16159

water, filtered, washed, dried, weighed, and resuspended in a 50% IPA mixture with Nafion. Pt loadings of samples prior to mixing with Nafion were determined by electron dispersive spectroscopy (EDS).[47] Some samples have the NaOH rinsing step omitted to determine the impact of alkaline rinses separately from the supporting procedure. For the commercial Pt−C catalyst investigated here (TKK), the Pt−C ink was fabricated according to the method outlined by Gasteiger et al.[51] and Garsany et al.[52] with 25% IPA.

Electrochemical Measurements. Several electrochemical assessments of each catalyst were made, including the electrochemically active surface area (ECA) by proton stripping for electrodes with different coverages of adsorbed Sn, cyclic voltammetry to determine the EOR peak potential, and chronoamperometry to determine the change in EOR activity over time.

Electrochemical Cell. All characterization was carried out in a standard three-electrode electrochemical cell with a Ag/AgCl reference electrode (connected via a potassium nitrate salt bridge to the main electrochemical cell) and a Pt-wire counter electrode. Measurements were conducted at room temperature. The rotating-disk electrode assembly, rotator, potentiostat, and software were purchased from Pine Instruments. Potentials in this article are referenced to the reversible hydrogen electrode (RHE). Calibration of the Ag/AgCl reference electrode was done by measuring the proton underpotential deposition region on an electrochemically cleaned polycrystalline Pt electrode (0.196 cm^2). The characteristic transition from this region to solvent reduction was placed at 0.05 V versus RHE. Electrodes were lowered under potential control into the electrochemical cell for each analysis at 0.2 V versus RHE. All characterization steps occurred with Pt−C ink electrodes fabricated on glassy-carbon disk electrodes (0.196 cm^2). Approximately 20 μL of C−Pt ink was pipetted onto the surface of a glassy-carbon (GC) rotating disk electrode (RDE) and dried under nitrogen with rotation at 400 rpm for 30 min.[53] Care was taken to use separate glassware for ECA and EOR assessments to prevent the contamination of ECA measurements with ethanol.

ECA Measurements by Proton Stripping. C−Pt electrodes were immersed in nitrogen-saturated 0.5 M sulfuric acid under potential control at 0.2 V and cycled from 0.05−0.67 at 0.05 V/s until a stable signal was achieved, ca. 40 cycles. The last sweep was used to determine the ECA by proton stripping in the presence of surface-adsorbed Sn. To determine the ECA for the Pt nanoparticles free of adsorbed Sn, the potential window was increased to 1.1 V and the electrodes were cycled until a stable signal was achieved. The Sn coverage, θ_{Sn}, could be determined by comparing the H_{UPD} stripping charge in the 0.05−0.4 V region for Sn-covered and Sn-free Pt nanoparticle surfaces using eq 1

$$\theta_{Sn} = 1 - \frac{Q_{Pt}(\text{Sn-covered})}{Q_{Pt}(\text{Sn-free})} \quad (1)$$

where Q_{Pt} is the charge determined via H_{UPD} stripping from the Pt surface. Determining Sn fraction in this way allows us to determine specific activities by normalizing the EOR current to the area of available Pt. This step is frequently omitted in the literature[10] but is nevertheless important for making comparisons between investigations and modeling kinetic data.[51,52]

The Sn-free proton stripping charge was determined electrochemically by removing all of the surface-adsorbed Sn by increasing the potential window used for ECA analysis to strip Sn from the surface anodically. The potential window was increased in 0.05 V increments until stable current measurements over several cycles were achieved. In no case did the potential window exceed 0.8 V for samples where residual Sn was maintained on the electrode. Fractional Sn coverages could be induced on the Pt surface electrochemically once the Sn-free charge had been determined.

EOR Voltammetry and Chronoamperometry Measurements. New electrodes were made and the Sn coverage was determined using proton stripping according to the method described above. Electrodes were then placed into nitrogen-saturated 0.5 M sulfuric acid with 0.5 M ethanol under potential control at 0.2 V and were swept to 0.67 V and then back to 0.2 at 0.05 V/s to determine the peak potential for the EOR. Following this sweep, the electrode potential was set to 0.42 V and held constant for 2 h. Electrode ECA was collected after chronoamperometic measurements to determine if there were changes in tin coverage. No changes in tin coverage were detected following EOR activity measurements in the acid electrolyte. An identical procedure was used to determine the activity in 0.1 M KOH, 0.5 M ethanol. A significant change in Sn coverage was detected following EOR in the alkaline electrolyte, as will be discussed.

Chemical Removal of Sn. Nonelectrochemical approaches were also used to remove surface-adsorbed Sn in order to demonstrate commercially applicable techniques for tin removal.[46,54] Here, C−Pt electrodes fabricated on glassy carbon electrodes were exposed for 15 min to concentrated hydrochloric acid, followed by copious rinsing with DI water. Following chemical exposure, ECA was determined using the method described above.

Raman Spectroscopy. Raman spectroscopy was used to identify the chemical composition of Sn in the electrodes. The particles were precipitated by neutralizing the as-fabricated Sn−Pt nanoparticle colloidal suspensions with excess NaOH. Then the nanoparticles were centrifuged and washed with DI water until the rinsate pH was neutral. All of the samples were dried overnight under vacuum at 100 °C. Raman spectra were obtained on dried nanoparticle samples for particles synthesized with different Sn/Pt ratios, namely, 2.5, 3, and 9. All Raman scattering measurements made use of a dispersive system (model T 64 000; Horiba, Jobin Yvon Inc.) using 514 nm excitation. The dispersive system made use of a microscope attachment with an 80× objective bringing laser light to a fine focus (1 μm spot size) and the scattered radiation detected using a charge-coupled device (CCD) detector.

Energy-Dispersive Spectroscopy. Pt nanoparticle assemblies in aluminum pans were analyzed by EDS (EDAX Corp.) in an FE-SEM (FEI XL-30 System) at the University of Cincinnati Materials Characterization Laboratory. EDS on the pan control sample exhibited a nearly 100% aluminum background signal having very low interference with Pt and Sn peak positions. The catalysts, after being supported on carbon but before mixing with Nafion, were deposited onto aluminum pans and attached by conductive carbon tape to a sample stage. Because the scattering volume penetrates a few micrometers, the entire thickness of the electrode was analyzed. Standardless quantitative analysis was performed at a constant acceleration potential of 15 keV, a working distance of 10 mm, an amp time of 51.2 μs (to maintain an optimum dead time of 30%), and a magnification of 200×. The C K-emission intensity was compared to the Pt M- and Sn L-emission intensities for relative analysis and carbon loading determination. At least three measurements per sample were taken.

X-ray Diffraction. X-ray diffraction (XRD) was used to characterize the particle size of the commercial nanoparticle sample. Approximately 1 g of the commercial C−Pt catalyst was packed into an aluminum holder approximately 1 cm^2 and 4 mm thick. Scattering measurements were made on a PW3040 X'Pert XRD station (Phillips) at the University of Cincinnati Materials Characterization Laboratory with a wavelength, λ, of 1.54 (Cu Kα). Contributions from the aluminum holder were absent from XRD patterns of C−Pt samples, indicating thick sample packing. The 2θ range investigated was 30−90°. Step sizes of 0.2° were used with an exposure time of 10 s at each step. XRD peaks were analyzed using the well-known Scherrer equation to determine the volume-averaged particle size D

$$D = \frac{K\lambda}{\text{fwhm}\cos\theta} \quad (2)$$

where K is the Scherrer constant (0.89), fwhm is the full width at half-maximum of the peak, and θ is the Bragg angle of the [hkl] reflection. Contributions from particle strain were neglected when determining the volume-averaged particle size here. However, Leontyev et al.[55] demonstrate a method for accounting for the grain strain when determining the volume-averaged particle size. The data were processed and the (111) peak was fit using Matlab R2011a with a three-parameter Gaussian to determine the fwhm and θ.

Table 1. Nanoparticles Investigated

	particle diameter		Sn surface coverage for indicated removal method, θ_{Sn}				
	STEM (nm ± std)[a]	$ECA_{Sn\text{-}free}$ (nm)	e-chem[c]	HCl[d]	e-chem	NaOH[e]	water[f]
C–Pt (Sn/Pt = 2.50)	2.75 ± 0.21	3.95	0	0.36	0.60	0.85	~0.99
C–Pt (Sn/Pt = 3.00)	1.72 ± 0.12	2.22	0	0.34	0.58	0.86	~0.99
C–Pt (Sn/Pt = 9.00)	0.6	1.61	0	0.35	0.56	0.84	~0.99
Vulcan C–Pt (TKK)	5.51[b]	5.10	0	N/A	N/A	N/A	N/A

[a]±1 standard deviation. [b]Determined from fits to XRD. [c]Tin removed by potential electrode cycling. [d]Tin removed by concentrated electrode washing. [e]Tin removed by NaOH during support. [f]Tin removed by water washes only during support.

RESULTS AND DISCUSSION

Nanoparticle Synthesis and Particle Size Characterization. The particle size was measured using ex situ HAADF-STEM and was compared to in situ size estimates from ECA analysis where an average spherical geometry was assumed. HAADF-STEM imaging for the noncommercial Pt nanoparticles synthesized has been reported previously.[45,47] The particles investigated here represent three nanoparticle structures previously described, namely, atomic clusters, amorphous transitional nanoparticles, and single-crystal nanoparticles. Sizes were determined from measurements of at least 100 particles in high-magnification HAADF-STEM images and are presented in Table 1. Differences in particle size between STEM/XRD and ECA results could be caused by irregular geometries or by small amounts of agglomeration caused by electrochemical cycling.

Chemical Composition of Sn Following Electrostatic Assembly. The chemical state of the adsorbed Sn was examined at various stages of chemical washing that occur during the process of supporting the nanoparticles on carbon. The nanoparticles were first examined following their precipitation with excess NaOH. The carbon and binding polymer were omitted in order to determine the chemical composition of Sn using Raman spectroscopy without interference from the support. The precipitated nanoparticles, when dried, formed small flakes that were suitable for dispersive Raman spectroscopy. The results are shown in Figure 1.

The observed line shapes of Figure 1 for the Sn ligand are consistent with nanometer-sized particles of crystalline SnO_2 (c-SnO_2) but with a relative increase in the contribution of surface modes. The weak, broad nature of the vibrational features observed in Figure 1 suggests 2D-like structure for the adsorbed SnO_x consistent with its ligand nature. The reference spectra have been included to show how the A_{1g} mode for the ligand is red-shifted versus bulk c-SnO_2. The red shift in the A_{1g} mode is compared in Figure 1 to those reported for bulk c-SnO_2 (>100 nm particle size) and for smaller SnO_2 nanoparticles (<50 nm particle size). One notes that as the c-SnO_2 particle size diameter, D, decreases from 100 to 4.5 nm, the vibrational modes of the rutile SnO_2 phase (473, 633, 694, and 775 cm^{-1}) steadily red shift and broaden with a consequent decrease in the scattering strength. The trend is consistent with the known phonon dispersion curves ($\omega(k)$) that show a decrease in mode frequency, ω, with an increase in the wave vector, k, of excitation. In bulk c-SnO_2, one probes the zone center phonons (i.e., $k \rightarrow 0$ limit) because the diameter is much greater than the lattice constant, ca. 0.35 nm.[57] However in the smaller nanoparticles and the SnO_x ligand on the Pt nanoparticles, one samples a steadily larger wave vector, $k = 2\pi/D$, with the result that one observes a red shift and mode broadening. In addition, the relative contribution of surface modes[56] (ca. 500, 560, and 585 cm^{-1}) increases in relation to the A_{1g} mode at ca. 633 cm^{-1}. This is consistent with a large increase in the surface-to-volume ratio of the SnO_x ligand on the Pt nanoparticle.

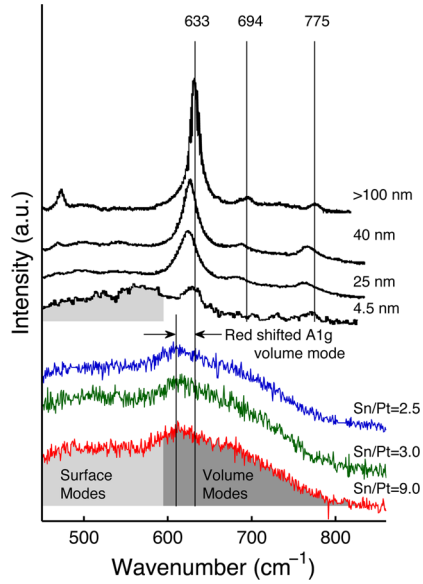

Figure 1. Dispersive Raman spectroscopy of precipitated Pt nanoparticles following washing in NaOH. The different Pt nanoparticle sizes are indicated by the Sn/Pt ratio in the synthesis solution: 2.5 (blue), 3.0 (green), and 9.0 (red). Reference spectra (black) have been included for different SnO_2 nanopowders investigated by Abello et al.,[56] where the nanoparticle size is given. Some volume mode peaks for crystalline SnO_2 are also labeled. The wavenumber ranges where surface and volume modes have been determined[56] are indicated. The relative contributions of the surface modes increase with decreasing SnO_2 nanopowder size. In addition, surface modes dominate the Raman spectra of the SnO_x ligand on the Pt nanoparticle. The presence of the A_{1g} mode at ca. 633 cm^{-1} for the SnO_x ligand suggests a tetragonal structure but is red-shifted and broadened versus crystalline SnO_2, as discussed in the text.

EDS data were collected on the supported Pt–C after electrostatic assembly and washing in NaOH to determine the Pt loading to look for residual contaminants such as Cl and Na and to corroborate the data from Raman spectroscopy. The relative loading was determined by comparing the Pt and C weight fractions determined from the K and M lines, respectively (Figure 2). The data indicate the complete removal of Cl with the distinct absence of the Cl Kα line at ca. 2.6 keV. The Pt M line increases with increasing particle size and is consistent with our previous work on the use of a cationic binder to assemble Pt nanoparticles on carbon electrostatically.[47] The Sn/Pt ratio increases with decreasing particle size

dx.doi.org/10.1021/la403704w | Langmuir 2013, 29, 16150–16159

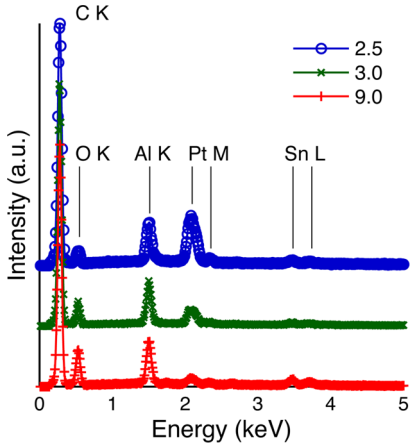

Figure 2. EDS results for the different supported nanoparticle catalysts investigated following the support on carbon and washing but prior to mixing with Nafion to form catalyst inks for the different particle sizes as indicated by the Sn/Pt ratio in the synthesis solution: 2.5 (blue), 3.0 (green), and 9.0 (red). The Pt peak increases with increasing particle size whereas the Sn peak increases with decreasing particle size. Both behaviors are consistent with electrostatic assembly with a surface-adsorbed Sn ligand.

as would be expected with the increase in the mass-specific surface area of the catalyst if Sn were a surface ligand.

Electrochemical Measurements of ECA, Sn Coverage, and EOR. Several electrochemical measurements were taken for various electrodes to determine the fractional Sn surface coverage, the EOR activity via chronoamperometry, and the EOR peak position and shape via cyclic voltammetry. The different electrodes investigated are listed in Table 1 on the basis of the fractional Sn surface coverage. Sn coverages are listed in the table as determined from integrating the H_{UPD} region and using eq 1. Proton stripping voltagrams are shown in Figure 3. The proton stripping behavior for Sn-covered surfaces are similar to other reports of the electrochemical removal of Sn from Pt surfaces.[19,46] A broad range of fractional Sn surface coverage was achieved. By limiting the scanning potential to 0.67 V during ECA, the scans were stable for 100 cycles, indicating no loss in surface Sn during cycling. In addition, scans taken following EOR measurements were identical to those taken before indicating an undetectable loss in surface Sn and the recovery of the Pt active area from CO_{ads} removal.

Chronoamperometry data (current density vs time measurements) were collected to investigate the ability of the Sn-covered Pt nanoparticles to resist surface poisoning by CO_{ads}. Results are shown in Figure 4. The current drops immediately after measurement begins and decreases over time. Surface kinetic processes control the EOR at 0.42 V because the potential is far from that needed to achieve diffusion-limited currents. Losses in current over time are therefore related to surface contamination by CO_{ads}. Table 2 gives the area- and mass-specific activities at 1 h.

All of the Sn-covered catalysts investigated exhibit dramatically enhanced performance versus the Pt-only commercial catalyst. The performance of the experimental catalysts exceeded those of commercial alloy catalysts (Pt–Ru, Johnson Matthey) and Pt–Sn alloy catalysts from literature reports.[3] The data in Table 2 illustrate a wide range of activities based on the Sn coverage with a maximum mass-averaged activity occurring with a fractional Sn surface coverage of about 0.6 in acidic electrolyte. The results for alkaline electrolyte are for Sn-free surfaces only because the adsorbed Sn ion was not stable and was removed from the surface after 1 h during chronoamperometry measurements. Each particle exhibited less than 5% Sn coverage at the end of the measurement. Attempts were not made to stabilize the Sn on the nanoparticle surface in alkaline electrolyte. The area-specific activity is compared to that of the best-performing Pt-only and Pt–Sn electrocatalysts under acidic and alkaline conditions in the bar chart of Figure 5 as a function of size. Except for the smallest nanoparticles, the area-specific activity of the custom-synthesized catalysts outperforms that of the commercial control catalyst in every case.

A comparable optimum Sn coverage was observed by El-Shafei et al.[18] on extended Pt(110) surfaces with adsorbed Sn whereas substantially lower maxima were observed with an optimum surface coverage of ca. 0.25 on (100) and (111) surfaces. Such similarity to our results suggests that our nanoparticle catalysts are dominated by Pt(110) active sites.[9] The Sn-free catalysts investigated here had surfaces nearly free of (111) surface terraces as determined by in situ electrochemical adatom studies. Instead, an increase in the fraction of five-coordinate (110) sites has been observed with increasing Pt nanoparticle size, and this may help explain the particle size effect observed in Figure 5. Attempts were made in the present work to use adatom stripping to determine the contributions from the various crystal facets on Pt in the presence of Sn. However, interference from the Sn stripping prevented the quantification of basal plane active sites, whereas weak stripping features from proton desorption prevented peak deconvolution by Lorentzian curve fitting.[58]

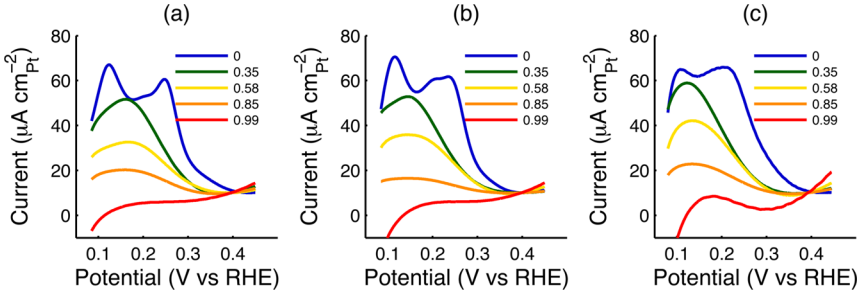

Figure 3. Electrochemical proton stripping behavior of the different catalysts in nitrogen-saturated 0.5 M sulfuric acid at several different average Sn surface fractions for the three different types of nanoparticles investigated: 0 (blue), 0.35 (green), 0.58 (yellow), 0.85 (orange), and 0.99 (red). Different particle sizes indicated by the Sn/Pt ratio in the synthesis solution: (a) 2.5, (b) 3.0, (c) and 9.0. The proton stripping behavior suggests that Sn is stripped uniformly from the surface as indicated by the fairly uniform increase in ECA with decreasing Sn coverage.

dx.doi.org/10.1021/la403704w | *Langmuir* 2013, 29, 16150–16159

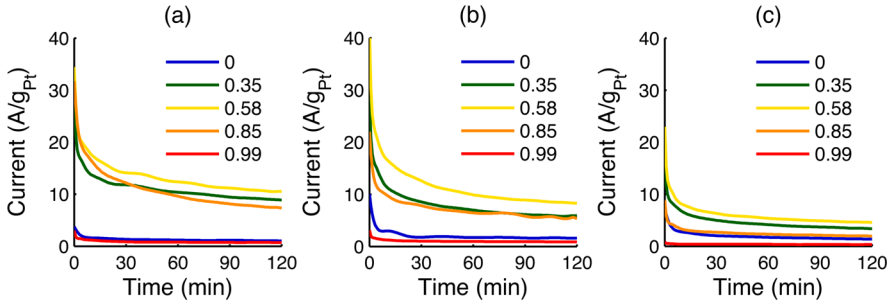

Figure 4. Chronoamperometry response in nitrogen-saturated 0.5 M ethanol, 0.5 M sulfuric acid at 0.42 V collected over 2 h at several different average Sn surface fractions: 0 (blue), 0.35 (green), 0.58 (yellow), 0.85 (orange), and 0.99 (red) as well as different particle sizes indicated by the Sn/Pt ratio in the synthesis solution: (a) 2.5, (b) 3.0, and (c) 9.0. The performance of the commercial data have been omitted for clarity.

Table 2. Area- and Mass-Specific Activities at 1 h Determined Using Chronoamperometry at 0.42 V

	area-specific activity (μA/cm$^2_{Pt}$)					mass-specific activity (A/g$_{Pt}$)				
avereage Sn coverage:	0	0.35	0.58	0.85	~0.99	0	0.35	0.58	0.85	~0.99
Acidic Electrolyte										
C−Pt (Sn/Pt = 2.50)	1.73	15.0	17.9	13.9	2.37	1.20	10.4	12.4	9.62	0.79
C−Pt (Sn/Pt = 3.00)	1.42	5.84	8.31	5.39	1.82	1.69	6.97	9.91	6.44	0.95
C−Pt (Sn/Pt = 9.00)	1.12	2.71	3.50	1.51	0.38	1.72	4.16	5.37	2.32	0.38
commercial C−Pt	1.89					1.02				
Alkaline Electrolyte										
C−Pt (Sn/Pt = 2.50)	6.64					4.60				
C−Pt (Sn/Pt = 3.00)	3.67					4.38				
C−Pt (Sn/Pt = 9.00)	1.77					2.71				
commercial C−Pt	3.16					1.70				

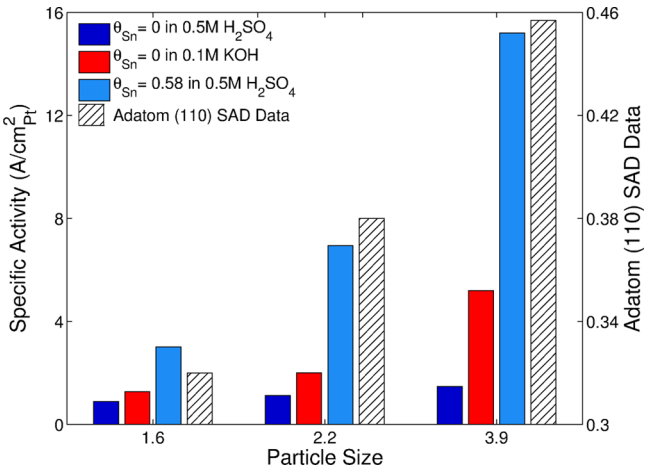

Figure 5. Comparison of area-specific activity (left) determined from chronoamperometry at 2 h for the best-performing catalysts under acidic and alkaline conditions with respect to Sn-free Pt nanoparticles in acid. Groups are labeled. The activity improves with increasing (110) surface fraction[9] (right) as discussed in the text. (ECA particle sizes are used.)

It should be noted that the surface energy of the Pt nanoparticles may be changed as a result of Sn adsorption, and one cannot preclude distortion of the underlying (110) active site. However, the predominance of (110)-like surface actives sites in acidic electrolyte where adsorbed Sn is stable is supported by the similar behavior observed on extended single-crystal electrodes.[18] The surface-averaged distribution (SAD) of Pt(110) sites for the particle sizes investigated is shown in Figure 5, and the corresponding ECA data is given in Table 1.

The observed particle size behavior is consistent with a new adlayer surface model that we have developed on the basis of our adatom investigations that indicate that nanoparticles have disordered surfaces dominated by (110) and (311) five-coordinate active sites.[9] Current data at 1 and 2 h measured in acidic electrolyte at several Sn coverages is shown in Figure 6. The SAD of Pt(110) sites is used to determine the active surface fraction in Figure 6b. The active area was determined by multiplying the Sn-free area of the catalyst surface determined using proton stripping with the SAD of Pt(110) sites. There is a correlation between the active area based on available Pt(110) sites and EOR activity.

The particle size effect is further evidenced by a close examination of the peak potential obtained during cyclic voltammetry during ethanol oxidation in an acidic electrolyte. The peak potential for EOR was compared to the work of Du et al.[3] The EOR results are shown in Figure 7 for the different electrodes investigated in both acidic and alkaline electrolytes. These results indicate a peak potential appearing at ca. 0.55 V for the several electrodes investigated in acidic electrolyte. A similar peak potential was not detected in the potential range investigated in alkaline electrolyte; however, the comparison of the data indicates a particle size effect in alkaline electrolyte and a reason for electrolyte-dependent performance differences consistent with literature reports[48,49] for the catalysts when chronoamperometry data are collected at 0.42 V. The similar shape of the peak between electrodes at the several Sn surface fractions in acidic electrolyte suggests the formation of the same product. By comparing to the results given by Du et al., the most likely product is acetaldehyde, which suggests that the oxidation is incomplete and the C−C bond is not broken.

A more detailed analysis of the EOR peak positions as a function of particle size in acidic electrolyte for the catalysts

dx.doi.org/10.1021/la403704w | Langmuir 2013, 29, 16150−16159

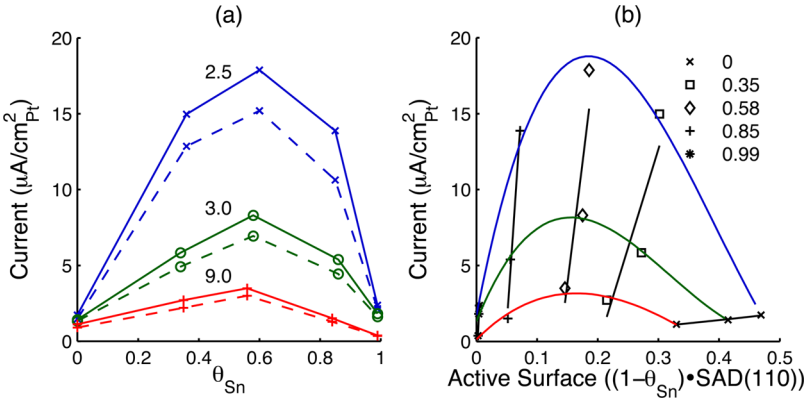

Figure 6. (a) Chronoamperometric area-specific activity of the catalysts synthesized here at 1 h (solid) and 2 h (dotted) in an acidic electrolyte for several particle sizes indicated by the Sn/Pt ratio in synthesis solution [2.5 (blue), 3.0 (green), and 9.0 (red)] as a function of Sn surface fraction. (b) The area specific activity at 1 h from part a plotted as a function of the active area determined by multiplying the Pt area $(1 - \theta_{Sn})$ by the SAD(110) area measured on Sn-free Pt surfaces for several particle sizes indicated by the Sn/Pt ratio in the synthesis solution: 2.5 (blue), 3.0 (green), and 9.0 (red). The results indicate a strong correlation between the active area and area-specific activity as well as a variation with the Sn surface fraction. The maximum activity occurs at a Sn surface fraction of about 0.6 for all of the catalysts investigated.

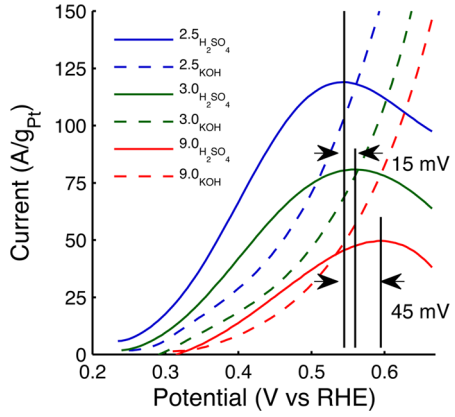

Figure 7. Cyclic voltammetric current response in nitrogen-saturated 0.5 M ethanol, 0.5 M sulfuric acid (solid lines) or 0.1 M KOH (dashed line) with a 0.05 V/s sweep rate at the optimum average Sn surface fraction of 0.58 in acidic electrolyte or Sn-free for alkaline electrolyte for the different particle sizes as indicated by the Sn/Pt ratio in the synthesis solution: 2.5 (blue), 3.0 (green), and 9.0 (red). The contribution of capacitive currents in ethanol-free electrolyte has been subtracted from the data presented here.

synthesized here indicates that the peak shifts to more anodic potentials as the particle size is reduced. The surface process captured by the peak in the CV data is the oxidation of acetaldehyde to acetic acid in the presence of adsorbed Sn.[3,59] The peak current response is dependent upon the concentration of the adsorbed intermediate, and the peak location is an indicator of how easily the CO_{ads} intermediates are hydrated and removed from the surface. The shift in the peak to lower potentials as the particle size increases indicates that surface poisoning is mitigated.[20,21,32,33] Such a shift may be due to an optimization of the surface site proximity between the Sn that activates the water and the Pt location where the acetaldehyde binds to the nanoparticle surface. Alternatively, the smallest particles have a high proportion of low-coordination edge and corner sites that may more strongly bind the CO_{ads} to the surface, preventing their oxidation by the adjacent OH_{ads} molecules until a sufficient anodic potential is achieved. This could be the source of the particle size effect observed in Figure 6.

The shape of the current response in alkaline electrolyte indicates a similar particle size effect that can be attributed to the same surface active site optimization responsible for the particle size effect in acidic electrolyte. However, under alkaline conditions, the half-wave potential for ethanol oxidation is not shifted to sufficiently anodic potentials to outperform the catalyst under acidic conditions at 0.42 V because of fundamentally different reaction mechanisms in the presence of surface-adsorbed Sn in acidic electrolyte and Sn-free surfaces in alkaline electrolyte. The particle size effect is not frequently reported in the literature for ethanol oxidation in alkaline electrolyte.[6] To the best of our knowledge, this is the first time that the particle size effect is attributed to a particular surface active site distribution determined in situ that is predominately stepped. Significantly, it has been demonstrated that the onset potential on stepped surfaces of ca. 0.42 V versus RHE is similar to the results demonstrated in Figure 7 for both acidic and alkaline catalysts.[43] Figure 5 shows that whereas Pt-only catalysts perform better under alkaline conditions at 0.42 V, the best EOR performance is achieved by the optimized Pt−Sn catalysts under acidic conditions.

Proposed Surface Model. Electrochemical stripping or chemical washing of Sn from Pt has been shown here to yield a systematic increase in the H_{UPD} area over the range of 0.05−0.4 V for all nanoparticle sizes investigated. In addition, the Raman data analysis shows emission spectra consistent with thin shells of Sn presumed to be on the surface of the Pt catalyst as evidenced by its surface active site blocking effects measured during H_{UPD} ECA determination. These observations are consistent with the uniform bonding of Sn on the Pt core. Such nonspecific interaction of the Sn ligand with the Pt core surface suggests that Sn can be uniformly stripped without preference for a particular EOR active site. This explains why we were able to observe a correlation between increasing nanoparticle size (with an associated increasing fraction of (110) sites on Sn-free Pt) and EOR activity across all Sn fractions investigated (Figure 5). Such uniform Sn removal also explains why the area-specific EOR activity of the surface exhibits a maximum with a fractional Sn surface coverage consistent with single-crystal Pt(110) data (a value of about 0.6).

A uniform surface site preference for adsorbed Sn can also be assessed from its stripping behavior as well as from the

dx.doi.org/10.1021/la403704w | Langmuir 2013, 29, 16150−16159

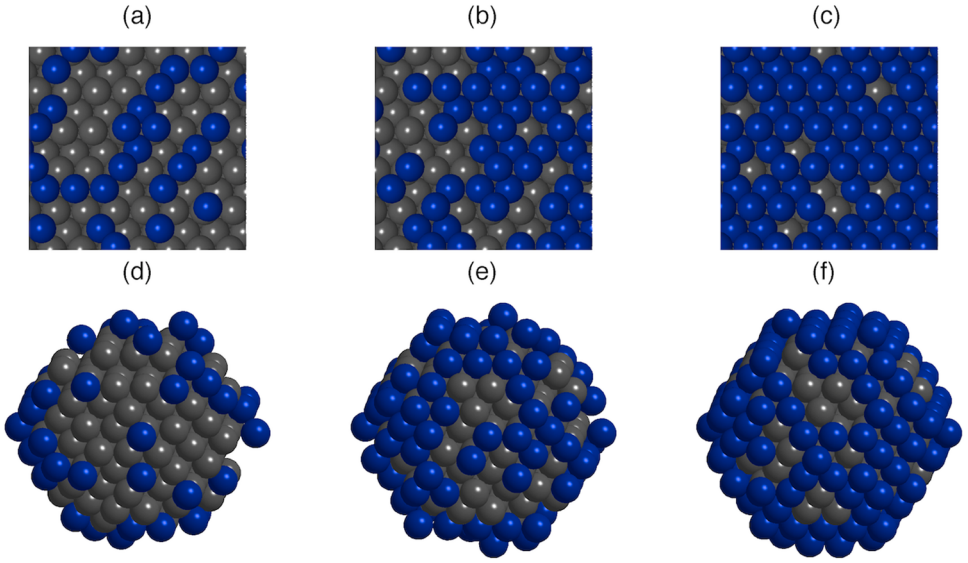

Figure 8. Pt(110) extended (top) or nanoparticle (bottom) surfaces with adsorbed Sn (blue). (a) 30, (b) 60, and (c) 90% Sn coverage on the extended Pt(110) surface. (d) 30, (e) 60, and (f) 90% Sn coverage on a 1.88-nm-diameter Pt nanoparticle surface with a high surface fraction of (110) sites developed using a new adlayer model. Sn has been packed as FCC Pt but at random surface locations. Surface fractions are approximate.

adsorption behavior of protons in the presence of Sn. Both reveal that Sn binds nonspecifically to the surface, in agreement with EXAFS data that we have recently collected.[60] First, anodic stripping of Sn from Pt surfaces occurs at ca. 0.6 V in acidic media with no systematic difference in stripping potential depending on the crystal plane.[11,17,18] Second, during Sn stripping the proton desorption peaks increase uniformly in the potential range of 0.05−0.4 V.[19,33]

Several authors have described the preferential adsorption of Sn to terrace hollow sites on Pt basal planes[11] or to trough sites on steps in the case of extended surfaces.[18,19] To reconcile these observations with the nonspecific Sn removal observed in our present study, we postulate that Sn adsorbs uniformly on the surface at trough sites, at terrace hollow sites, and on low-coordination edge and corners consistent with FCC packing (i.e., not at bridge locations). Figure 8a−c shows Sn atoms distributed randomly over an extended Pt(110) surface whereas Figure 8d−f shows Sn atoms distributed randomly over the surface of a Pt surface dominated by (110) and (311) planes. This model accounts for the structure-sensitive (Pt(110) fraction-dependent) catalytic activity that has been observed on these materials as a result of the uniform removal of Sn atoms from the surface.

CONCLUSIONS

A unique method for producing Pt nanoparticles with a uniform adsorbed layer of Sn has been used here independently to investigate the impact of Sn surface coverage and the underlying active site distribution on electrocatalytic EOR. Sn serves as both a reducing and stabilizing agent and thereby permits the fine discrimination of particle size and the associated active site distribution at the onset of nanoparticle formation of ca. 1−3 nm. Our work was motivated by a need to understand the impact of both the Sn promoter coverage and the particle size in dispersed nanoparticle systems as a means of optimizing the EOR under acidic and alkaline conditions.

Using Raman spectroscopy, we have demonstrated that Sn forms a uniform thin shell of 2D SnO_x on the Pt surface. The oxide is known to promote the oxidation of CO_{ads} and facilitate its removal from the Pt surface. This is primarily achieved by the oxidation of acetaldehyde to acetic acid. The CV results suggest that the oxidation product is acetic acid. Overall, the system investigated demonstrates remarkable ethanol oxidation activity versus Pt-only catalysts and Pt−Sn catalysts previously reported in the literature. We have achieved a significant systematic alteration of both mass-specific and area-specific activity with particle size (active site distribution) and Sn coverage. The results indicate that the optimum fraction coverage of Sn on Pt nanoparticles for alcohol oxidation is approximately 0.6 and that the EOR activity increases with particle size. The active site on the particles is associated with five-coordinate Pt(110) and Pt(311) on the basis of comparison with single-crystal data and active site determination on Sn-free Pt nanoparticles. The resultant electrocatalyst has a substantially higher EOR activity under acidic conditions than either bi- or trimetallic commercial systems or Pt-only catalysts under alkaline conditions. This result indicates that the mitigation of intermediate poisoning is more important to optimizing EOR activity on Pt nanoparticle catalysts than the type of electrolyte employed.

AUTHOR INFORMATION

Corresponding Author

*E-mail: anastasios.angelopoulos@uc.edu.

Author Contributions

The manuscript was written through the contributions of all authors. All authors have given approval to the final version of the manuscript.

Notes

The authors declare no competing financial interest.

ACKNOWLEDGMENTS

We express our appreciation to Jon Glandorf and James Lucas, undergraduate students at the University of Cincinnati, for rotating disk electrode measurements collected during the summer of 2011. Graduate student (S.S.J.) support was provided by the University of Cincinnati Graduate School. Support for both graduate (S.S.J.) and undergraduate (Jon

Glandorf and James Lucas) students was provided by an NSF REU Site Grant for Sustainable Urban Environments (grant no. EEC-1004623).

REFERENCES

(1) Vigier, F.; Coutanceau, C.; Perrard, A.; Belgsir, E. M.; Lamy, C. Development of Anode Catalysts for a Direct Ethanol Fuel Cell. *J. Appl. Electrochem.* **2004**, *34*, 439−446.
(2) Kowal, A.; Li, M.; Shao, M.; Sasaki, K.; Vukmirovic, M.; Zhang, J.; Marinkovic, N.; Liu, P.; Frenkel, A.; Adzic, R. R. Ternary Pt/Rh/SnO_2 Electrocatalysts for Oxidizing Ethanol to CO_2. *Nat. Mater.* **2009**, *8*, 325−330.
(3) Du, W.; Wang, Q.; Saxner, D.; Deskins, N. A.; Su, D.; Krzanowski, J. E.; Frenkel, A. I.; Teng, X. Highly Active Iridium/Iridium-Tin/Tin Oxide Heterogeneous Nanoparticles as Alternative Electrocatalysts for the Ethanol Oxidation Reaction. *J. Am. Chem. Soc.* **2011**, *133*, 15172−15183.
(4) Markovic, N.; Gasteiger, H.; Ross, P. N. Kinetics of Oxygen Reduction on Pt(hkl) Electrodes: Implications for the Crystallite Size Effect with Supported Pt Electrocatalysts. *J. Electrochem. Soc.* **1997**, *144*, 1591−1597.
(5) Markovic, N. M.; Gasteiger, H. A.; Ross, P. N. Oxygen Reduction on Platinum Low-Index Single-Crystal Surfaces in Alkaline Solution: Rotating Ring $Disk_{Pt(hkl)}$ Studies. *J. Phys. Chem.* **1996**, *100*, 6715−6721.
(6) Spendelow, J. S.; Wieckowski, A. Electrocatalysis of Oxygen Reduction and Small Alcohol Oxidation in Alkaline Media. *Phys. Chem. Chem. Phys.* **2007**, *9*, 2654−2675.
(7) Fujiwara, N.; Siroma, Z.; Yamazaki, S.-i.; Ioroi, T.; Senoh, H.; Yasuda, K. Direct Ethanol Fuel Cells Using an Anion Exchange Membrane. *J. Power Sources* **2008**, *185*, 621−626.
(8) Nesselberger, M.; Ashton, S.; Meier, J. C.; Katsounaros, I.; Mayrhofer, K. J. J.; Arenz, M. The Particle Size Effect on the Oxygen Reduction Reaction Activity of Pt Catalysts: Influence of Electrolyte and Relation to Single Crystal Models. *J. Am. Chem. Soc.* **2011**, *133*, 17428−17433.
(9) St. John, S.; Angelopoulos, A. P. In Situ Analysis of Optimum Surface Atom Coordination for Pt Nanoparticle Oxygen Reduction Electrocatalysts. *Electrochim. Acta* **2013**, *112*, 258−268.
(10) Wang, Y.; Song, S.; Andreadis, G.; Liu, H.; Tsiakaras, P. Understanding the Electrocatalytic Activity of PtxSny in Direct Ethanol Fuel Cells. *J. Power Sources* **2011**, *196*, 4980−4986.
(11) Zheng, Q. W.; Fan, C. J.; Zhen, C. H.; Zhou, Z. Y.; Sun, S. G. Irreversible Adsorption of Sn Adatoms on Basal Planes of Pt Single Crystal and Its Impact on Electrooxidation of Ethanol. *Electrochim. Acta* **2008**, *53*, 6081−6088.
(12) Zhou, W. P.; Axnanda, S.; White, M. G.; Adzic, R. R.; Hrbek, J. Enhancement in Ethanol Electrooxidation by SnOx Nanoislands Grown on Pt (111): Effect of Metal Oxide−Metal Interface Sites. *J. Phys. Chem. C* **2011**, *115*, 16467−16473.
(13) Kita, H.; Shimazu, K.; Kunimatsu, K. Electrochemical Oxidation of CO on Pt in Acidic and Alkaline Solutions: Part I. Voltammetric Study on the Adsorbed Species and Effects of Aging and Sn (IV) Pretreatment. *J. Electroanal. Chem. Interfacial Electrochem.* **1988**, *241*, 163−179.
(14) Scott, F. J.; Mukerjee, S.; Ramaker, D. E. Contrast in Metal−Ligand Effects on PtnM Electrocatalysts with M Equal Ru Vs Mo and Sn as Exhibited by in Situ XANES and EXAFS Measurements in Methanol. *J. Phys. Chem. C* **2009**, *114*, 442−453.
(15) Jiang, L.; Sun, G.; Sun, S.; Liu, J.; Tang, S.; Li, H.; Zhou, B.; Xin, Q. Structure and Chemical Composition of Supported Pt-Sn Electrocatalysts for Ethanol Oxidation. *Electrochim. Acta* **2005**, *50*, 5384−5389.
(16) Jiang, L.; Colmenares, L.; Jusys, Z.; Sun, G.; Behm, R. Ethanol Electrooxidation on Novel Carbon Supported Pt/SnO_XC Catalysts with Varied Pt: Sn Ratio. *Electrochim. Acta* **2007**, *53*, 377−389.
(17) Mukerjee, S.; McBreen, J. An in Situ X-ray Absorption Spectroscopy Investigation of the Effect of Sn Additions to Carbon-Supported Pt Electrocatalysts: Part I. *J. Electrochem. Soc.* **1999**, *146*, 600−606.
(18) El-Shafei, A. A.; Eiswirth, M. Electrochemical Activity of Sn-Modified Pt Single Crystal Electrodes for Ethanol Oxidation. *Surf. Sci.* **2010**, *604*, 862−867.
(19) Sobkowski, J.; Franaszczuk, K.; Piasecki, A. Influence of Tin on the Oxidation of Methanol on a Platinum Electrode. *J. Electroanal. Chem.* **1985**, *196*, 145−156.
(20) Frelink, T.; Visscher, W.; van Veen, J. A. R. The Effect of Sn on Pt/C Catalysts for the Methanol Electro-Oxidation. *Electrochim. Acta* **1994**, *39*, 1871−1875.
(21) Frelink, T.; Visscher, W.; van Veen, J. A. R. On the Role of Ru and Sn as Promotors of Methanol Electro-Oxidation over Pt. *Surf. Sci.* **1995**, *335*, 353−360.
(22) Panja, C.; Saliba, N.; Koel, B. Adsorption of Methanol, Ethanol and Water on Well-Characterized Pt—Sn Surface Alloys. *Surf. Sci.* **1998**, *395*, 248−259.
(23) Neto, A.; Dias, R.; Tusi, M.; Linardi, M.; Spinace, E. Electro-Oxidation of Methanol and Ethanol Using PtRu/C, PtSn/C and PtSnRu/C Electrocatalysts Prepared by an Alcohol-Reduction Process. *J. Power Sources* **2007**, *166*, 87−91.
(24) Lim, D. H.; Choi, D. H.; Lee, W. D.; Lee, H. I. A New Synthesis of a Highly Dispersed and CO Tolerant PtSn/C Electrocatalyst for Low-Temperature Fuel Cell; Its Electrocatalytic Activity and Long-Term Durability. *Appl. Catal. B* **2009**, *89*, 484−493.
(25) Manzo-Robledo, A.; Boucher, A. C.; Pastor, E.; Alonso-Vante, N. Electro-Oxidation of Carbon Monoxide and Methanol on Carbon-Supported Pt−Sn Nanoparticles: A DEMS Study. *Fuel Cells* **2002**, *2*, 109−116.
(26) Boucher, A. C.; Alonso-Vante, N.; Dassenoy, F.; Vogel, W. Structural and Electrochemical Studies of Pt-Sn Nanoparticulate Catalysts. *Langmuir* **2003**, *19*, 10885−10891.
(27) Melke, J.; Schoekel, A.; Dixon, D.; Cremers, C.; Ramaker, D. E.; Roth, C. Ethanol Oxidation on Carbon-Supported Pt, PtRu, and PtSn Catalysts Studied by Operando X-ray Absorption Spectroscopy. *J. Phys. Chem. C* **2010**, *114*, 5914−5925.
(28) Gupta, S. S.; Singh, S.; Datta, J. Promoting Role of Unalloyed Sn in PtSn Binary Catalysts for Ethanol Electro-Oxidation. *Mater. Chem. Phys.* **2009**, *116*, 223−228.
(29) Lim, D. H.; Choi, D. H.; Lee, W. D.; Park, D. R.; Lee, H. I. The Effect of Sn Addition on a Pt/C Electrocatalyst Synthesized by Borohydride Reduction and Hydrothermal Treatment for a Low-Temperature Fuel Cell. *Electrochem. Solid-State Lett.* **2007**, *10*, B87−B90.
(30) Jones, F. E.; Milne, S. B.; Gurau, B.; Smotkin, E. S.; Stock, S. R.; Lukehart, C. Synthesis and Characterization of PtSn/Carbon and Pt3Sn/Carbon Nanocomposites as Methanol Electrooxidation Catalysts. *J. Nanosci. Nanotechnol.* **2002**, *2*, 81−87.
(31) Joo, J. B.; Kim, Y. J.; Kim, W.; Kim, P.; Yi, J. Preparation and Characterization of a PtSn Nanocatalyst for Use in Ethanol Electro-Oxidation. *J. Nanosci. Nanotechnol.* **2008**, *8*, 5130−5134.
(32) Morimoto, Y.; Yeager, E. B. Co Oxidation on Smooth and High Area Pt, Pt-Ru and Pt-Sn Electrodes. *J. Electroanal. Chem.* **1998**, *441*, 77−81.
(33) Morimoto, Y.; Yeager, E. B. Comparison of Methanol Oxidations on Pt, Pt|Ru and Pt|Sn Electrodes. *J. Electroanal. Chem.* **1998**, *444*, 95−100.
(34) Anderson, A. B.; Seong, S.; Grantscharova, E. Molecular Orbital Investigation of Water Reactions with Tin Hydroxide Complexes in Association with Platinum Electrodes. *J. Phys. Chem.* **1996**, *100*, 17535−17538.
(35) Lamy-Pitara, E.; Ouazzani-Benhima, L. E.; Barbier, J.; Cahoreau, M.; Caisso, J. Adsorption of Tin on Platinum: An Uncommon Underpotential Deposition. *J. Electroanal. Chem.* **1994**, *372*, 233−242.
(36) Ishikawa, Y.; Liao, M. S.; Cabrera, C. R. Energetics of H_2O Dissociation and CO_{ads}+ OH_{ads} Reaction on a Series of Pt-M Mixed Metal Clusters: A Relativistic Density-Functional Study. *Surf. Sci.* **2002**, *513*, 98−110.

(37) Anderson, A. B.; Grantscharova, E.; Seong, S. Systematic Theoretical Study of Alloys of Platinum for Enhanced Methanol Fuel Cell Performance. *J. Electrochem. Soc.* **1996**, *143*, 2075−2082.
(38) Xu, Z.-F.; Wang, Y. Effects of Alloyed Metal on the Catalysis Activity of Pt for Ethanol Partial Oxidation: Adsorption and Dehydrogenation on Pt_3M (M = Pt, Ru, Sn, Re, Rh, and Pd). *J. Phys. Chem. C* **2011**, *115*, 20565−20571.
(39) Ishikawa, Y.; Liao, M. S.; Cabrera, C. R. Oxidation of Methanol on Platinum, Ruthenium and Mixed Pt−M Metals (M = Ru, Sn): A Theoretical Study. *Surf. Sci.* **2000**, *463*, 66−80.
(40) Liu, P.; Logadottir, A.; Nørskov, J. K. Modeling the Electro-Oxidation of CO and H_2/CO on Pt, Ru, PtRu and Pt_3Sn. *Electrochim. Acta* **2003**, *48*, 3731−3742.
(41) Li, M.; Cullen, D. A.; Sasaki, K.; Marinkovic, N. S.; More, K.; Adzic, R. R. Ternary Electrocatalysts for Oxidizing Ethanol to Carbon Dioxide: Making IR Capable of Splitting C−C Bond. *J. Am. Chem. Soc.* **2012**, *135*, 132−141.
(42) Li, M.; Kowal, A.; Sasaki, K.; Marinkovic, N.; Su, D.; Korach, E.; Liu, P.; Adzic, R. R. Ethanol Oxidation on the Ternary Pt−Rh−SnO_2/C Electrocatalysts with Varied Pt:Rh:Sn Ratios. *Electrochim. Acta* **2010**, *55*, 4331−4338.
(43) Braunchweig, B.; Hibbitts, D.; Neurock, M.; Wieckowski, A. Electrocatalysis: A Direct Alcohol Fuel Cell and Surface Science Perspective. *Catal. Today* **2013**, *202*, 197−209.
(44) Li, M.; Zhou, W. P.; Marinkovic, N. S.; Sasaki, K.; Adzic, R. R. The Role of Rhodium and Tin Oxide in the Platinum-Based Electrocatalysts for Ethanol Oxidation to CO_2. *Electrochim. Acta* **2013**, *104*, 454−461.
(45) St. John, S.; Dutta, I.; Angelopoulos, A. P. Synthesis and Characterization of Electrocatalytically Active Platinum Atom Clusters and Monodisperse Single Crystals. *J. Phys. Chem. C* **2010**, *114*, 13515−13525.
(46) St. John, S.; Lee, D.; Dutta, I.; Angelopoulos, A. P. Acceleration of Electrocatalytic Activity on Pt–Sn Nanoparticles. *J. Electrochem. Soc.* **2010**, *157*, B1245−B1250.
(47) St. John, S.; Dutta, I.; Angelopoulos, A. P. Enhanced Electrocatalytic Oxygen Reduction through Electrostatic Assembly of Pt Nanoparticles onto Porous Carbon Supports from $SnCl_2$-Stabilized Suspensions. *Langmuir* **2011**, *27*, 5781−5791.
(48) Lai, S. C. S.; Koper, M. T. M. The Influence of Surface Structure on Selectivity in the Ethanol Electro-Oxidation Reaction on Platinum. *J. Phys. Chem. Lett.* **2010**, *1*, 1122−1125.
(49) Lai, S. C. S.; Kleijn, S. E. F.; Öztürk, F. T. Z.; van Rees Vellinga, V. C.; Koning, J.; Rodriguez, P.; Koper, M. T. M. Effects of Electrolyte pH and Composition on the Ethanol Electro-Oxidation Reaction. *Catal. Today* **2010**, *154*, 92−104.
(50) Cohen, R. L.; West, K. W. Generative and Stabilizing Processes in Tin-Palladium Sols and Palladium Sol Sensitizers. *J. Electrochem. Soc.* **1973**, *120*, 502−508.
(51) Gasteiger, H. A.; Kocha, S. S.; Sompalli, B.; Wagner, F. T. Activity Benchmarks and Requirements for Pt, Pt-Alloy, and Non-Pt Oxygen Reduction Catalysts for Pemfcs. *Appl. Catal. B* **2005**, *56*, 9−35.
(52) Garsany, Y.; Baturina, O. A.; Swider-Lyons, K. E.; Kocha, S. S. Experimental Methods for Quantifying the Activity of Platinum Electrocatalysts for the Oxygen Reduction Reaction. *Anal. Chem.* **2010**, *82*, 6321−6328.
(53) Garsany, Y.; Singer, I. L.; Swider-Lyons, K. E. Impact of Film Drying Procedures on RDE Characterization of Pt/VC Electrocatalysts. *J. Electroanal. Chem.* **2011**, *662*, 396−406.
(54) Horkans, J.; Kim, J.; McGrath, C.; Romankiw, L. T. A TEM Study of the Effect of Accelerators on Pd-Sn Colloidal Catalysts and on the Initiation of Electroless Cu Deposition on Epoxy. *J. Electrochem. Soc.* **1987**, *134*, 300−304.
(55) Leontyev, I. N.; Belenov, S. V.; Guterman, V. E.; Haghi-Ashtiani, P.; Shaganov, A. P.; Dkhil, B. Catalytic Activity of Carbon-Supported Pt Nanoelectrocatalysts. Why Reducing the Size of Pt Nanoparticles Is Not Always Beneficial. *J. Phys. Chem. C* **2011**, *115*, 5429−5434.
(56) Abello, L.; Bochu, B.; Gaskov, A.; Koudryavtseva, S.; Lucazeau, G.; Roumyantseva, M. Structural Characterization of Nanocrystalline SnO_2 by X-ray and Raman Spectroscopy. *J. Solid State Chem.* **1998**, *135*, 78−85.
(57) Cheng, B.; Russell, J. M.; Shi; Zhang, L.; Samulski, E. T. Large-Scale, Solution-Phase Growth of Single-Crystalline SnO_2 Nanorods. *J. Am. Chem. Soc.* **2004**, *126*, 5972−5973.
(58) Solla-Gullón, J.; Rodriguez, P.; Herrero, E.; Aldaz, A.; Feliu, J. Surface Characterization of Platinum Electrodes. *Phys. Chem. Chem. Phys.* **2008**, *10*, 1359−1373.
(59) He, Q.; Shyam, B.; Nishijima, M.; Yang, X.; Koel, B.; Ernst, F.; Ramaker, D.; Mukerjee, S. Highly Stable Pt−Au@Ru/C Catalyst Nanoparticles for Methanol Electro-Oxidation. *J. Phys. Chem. C* **2013**, *117*, 1457−1467.
(60) St. John, S.; Angelopoulos, A. P. Submitted.